Determination of optical fiber parameters based on fiber gratings and a search procedure

Guolu Yin, Jian Tang, Changrui Liao, Jun He, Bing Sun, Guanjun Wang, and Yiping Wang

Abstract—**We demonstrated a new method to determine the optical fiber parameters using long period fiber gratings and a search procedure. The gratings with different pitches were inscribed to measure experimental phase matching curves. The theoretical phase matching curves were found by calculating the effective refractive indices of fiber modes. In the search procedure, the optical fiber parameters were varied in order to minimize the difference between the experimental phase matching curves and the theoretical ones. The optical fiber parameters were finally determined as long as the smallest difference value was reached.**

Index Terms—**Long period fiber grating, Optical fiber parameters, Search procedure**

I. INTRODUCTION

OPTICAl fiber parameters, e.g., fiber core radius, dopant concentration, and refractive index (RI), are crucial to determine the optical characteristics of the optical fibers. Knowing fiber parameters helps in designing and modeling fiber devices. Interference microscopy and the fundamental mode near-filed method are popular in determining the RI in optical fibers [1, 2]. Fiber gratings also have been employed to infer the RI or effective refractive index (ERI) in various kinds of optical fibers. L. Wang et al. characterized the ERIs of the vector modes in an orbital angular momentum fiber by measuring the Bragg wavelengths of fiber Bragg gratings [3]. S. Ramachandran measured the ERI separation between degenerated vector modes by lifting the polarization degeneracy with mechanically induced micro-bend long period fiber gratings (LPFGs) [4]. Y. J. Kim et al. measured the RI variation with temperature by use of LPFGs [5]. C. Schulze et al. measured the ERI difference in a multimode optical fiber at the resonant wavelength of a mechanical LPFG [6][7]. However, the above techniques only provide results at a single probe wavelength. Therefore, the material dispersion property can only be obtained by repeating measurements at numerous discrete wavelengths [8].

In this work, we have described a new method to determine

All authors are with Key Laboratory of Optoelectronic Devices and Systems of Ministry of Education and Guangdong Province, College of Optoelectronic Engineering, Shenzhen University, Shenzhen 518060, China (e-mail: ypwang@szu.edu.cn)

Guolu Yin is also with Aston Institute of Photonic Technologies, Aston University, Birmingham, B4 7ET, U.K. (e-mail: guoluyin@gmail.com)

the fiber parameters over a large wavelength range via a comparison between the optical properties of LPFGs inscribed in the fiber and modeling of these properties. In Section II, we fabricated a series of LPFGs with different grating pitches, determined the mode orders at the resonant wavelengths and constructed the experimental phase matching curves. In Section III, we presented the principle of a search procedure for determining the fiber parameters and defined the average absolute deviation of the resonant wavelengths for evaluating the difference between measured phase matching curves and the calculated ones. In section IV, we numerically calculated phase matching curves at different core index and core radius using a finite difference method, and constructed a procedure to search the fiber parameters for the ones that minimized the difference between the measured phase matching curves and the calculated ones. The optical fiber parameters were finally determined as long as the smallest difference value was reached. In Section V, we verified the correctness of the reconstructed optical fiber parameters by comparing the calculated effective group refractive indices and the typical values in the fiber datasheet.

II. INSCRIBING LPFGS

In this research, we determined the fiber core radius and the dopant concentration of a single mode optical fiber (FuIIBand® Plus Low Loss single mode fiber) from the Yangtze Optical Fiber and Cable Co., Ltd. In this fiber. We fabricated 40 LPFGs with different grating pitches using our proposed arc discharge technique [9-11]. The arc current and arc duration were fixed to be 13 mA and 6 s. The grating pitches varied from 360 μm to 750 μm with an interval of 10 μm, which was controlled by using a motorized translation stage with a precision of 10 nm. The shortest period of 360 μm is comparable with the value of 345 μm reported elsewhere [12].The small difference may be caused by the use of different electrodes in the respective experiments.
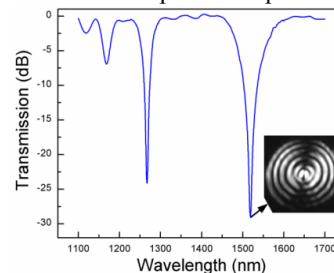

Fig. 1 Experimentally measured transmission spectrum of LPFG with grating pitch of 450 μm. Inset: measured near mode field at resonate dip 1518.7 nm

Table I. Measured resonant wavelengths (λ^{MRW}) corresponding to LP$_{12}$ — LP$_{17}$ cladding modes in LPGs

No.	Λ (μm)	Experimental resonant wavelength (nm)						No.	Λ (μm)	Experimental resonant wavelength (nm)			
		LP$_{17}$	LP$_{16}$	LP$_{15}$	LP$_{14}$	LP$_{13}$	LP$_{12}$			LP$_{15}$	LP$_{14}$	LP$_{13}$	LP$_{12}$
1	360	1362.88						21	560	1617.80	1389.68	1294.76	1240.52
2	370	1431.06	1180.6					22	570	1675.76	1415.12	1313.6	1260.56
3	380	1562.38	1216.86					23	580		1424.24	1318.88	1263.44
4	390		1251.86	1135.10				24	590		1446.08	1335.80	1278.8
5	400		1280.56	1149.24	1090.98			25	600		1469.36	1352.84	1290.21
6	410		1326.48	1172.76	1101.92			26	610		1480.28	1367.24	1296.44
7	420		1363.86	1197.54	1119.42			27	620		1503.68	1376.84	1314.08
8	430		1407.12	1220.08	1137.62			28	630		1513.68	1382.8	1314.96
9	440		1469.56	1249.21	1155.82			29	640		1534.41	1396.32	1326.10
10	450		1518.72	1266.98	1167.58			30	650		1554.10	1408.32	1336.2
11	460		1596.26	1293.32	1189.42	1133.28		31	660		1577.12	1424.63	1347.21
12	470		1671.44	1318.64	1204.12	1146.58		32	670		1599.08	1442.12	1363.43
13	480			1344.54	1220.22	1158.34	1127.54	33	680		1616.21	1449.32	1371.48
14	490			1377.86	1242.48	1174.16	1138.32	34	690		1634.96	1459.88	1376.96
15	500			1412.36	1264.88	1190.72	1150.01	35	700		1657.52	1475.84	1391.48
16	510			1434.25	1278.44	1212.56	1162.31	36	710		1678.64	1486.42	1400.36
17	520			1480.88	1309.76	1229.12	1174.64	37	720		1697.36	1496.48	1402.42
18	530			1515.56	1335.92	1246.52	1194.84	38	730			1510.22	1414.16
19	540			1541.96	1345.04	1258.04	1211.96	39	740			1523.61	1423.04
20	550			1576.68	1367.48	1277.48	1227.68	40	750			1530.56	1436.84

The transmission spectra of 40 gratings are experimentally measured by employing a supercontinuum white light source (NKT Photonics SuperK) and an optical spectrum analyser (OSA, YOKOGAWA AQ6370C) with a resolution of 0.02 nm. All 40 gratings have clear spectra with a maximum dip attenuation of ~30 dB and a low insertion loss of ~0.2 dB. Fig. 1 shows a typical measured transmission spectrum of LPFG with grating pitch of 450 μm. According to the transmission spectra, we recorded all measured resonant wavelengths of 40 gratings, summarizing in Table I.

In order to identify the mode orders of the resonant dips, we measured the near mode filed patterns at the resonant dips by employing a near-infrared camera and a tunable laser (Agilent, 81960A) with a wavelength range from 1505 to 1630 nm. In this experiment, one end of the LPFG sample was connected to the tunable laser, and the other end was cleaved at the last grating period. When the wavelength of the tunable laser was locked at the resonant dip of the LPFG, the majority amount of the LP$_{01}$ core mode power was transferred to the cladding mode, at which point a near mode field pattern of the cladding mode was observed in the camera. The inset of Fig.1 shows the near mode filed at the resonant wavelength of 1518.72 nm. The intensity distribution of the near mode field pattern indicates that the cladding mode order is LP$_{16}$ in terms of the number of the radial lobes throughout the entire cladding region [13]. It is inferred that the arc discharge-induced gratings couple light into the antisymmetric cladding modes LP$_{1m}$, where m is the radial cladding mode order.

As for the resonant dip, which is located outside the tunable wavelength range, the corresponding cladding mode order can't be directly determined by measuring the near mode filed pattern, but can be predicted from the known cladding mode order. For the LPFG with a certain grating pitch, the longer the wavelength where the resonant dip is located, the larger the radial cladding mode order. When the grating pitch gradually decreases, the new resonant dip corresponding to a higher radial cladding mode order arises at a longer wavelength range. Based on the principles above, six cladding mode orders were deduced sequentially to be LP$_{12}$, LP$_{13}$, LP$_{14}$, LP$_{15}$, LP$_{16}$, and LP$_{17}$ as shown in Table I.
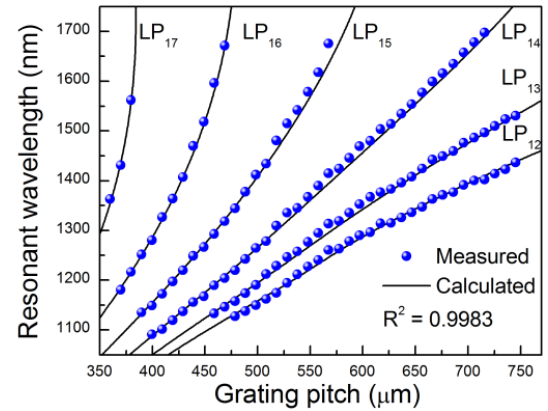

Fig. 2 Phase matching curves. Symbols: measured result, solid line: calculated result at r_{co} = 4.18 μm and C$_{GeO2}$ = 2.72%.

According to the cladding mode orders above, we categorized the resonant wavelengths of the ith LPFG sample, where i is the number of the grating and varies from 1 to 40. Next, we plotted the experimental resonant wavelengths as a function of the grating pitch, as shown in Fig. 2. Here, we only plotted six phase matching curves corresponding to LP$_{12}$, LP$_{13}$, LP$_{14}$, LP$_{15}$, LP$_{16}$, and LP$_{17}$. In fact, the light also coupled from the core mode to the LP$_{11}$ cladding mode, but the resonant dip for the LP$_{11}$ cladding mode was hardly distinguishable from the background noise, and the resonant wavelength could not be measured exactly. In order to minimize the influence of the measured resonant wavelengths on the determination of fiber parameters, we ignored the curve corresponding to the LP$_{11}$ cladding mode in Fig. 2.

III. PRINCIPLE OF THE SEARCH PROCEDURE

In order to model the theoretical resonant wavelengths, phase matching equation [14-17] has been successfully employed for measuring the RI variation with temperature based on KrF excimer laser induced LPFG [5] and measuring the ERI difference in few mode fibers based on mechanically induced LPFG [6]. In our theoretical model, the phase matching equation was expressed as a function of the fiber parameters, and the resonant wavelength of arc discharge induced LPFG can be estimated as follows:

$$\lambda_{im}^{CRW}\left(r_{co}, C_{GeO_2}\right) = \left(n_{01}^{co} - n_{1m}^{cl}\right)\Lambda_i = \Delta n_{01-1m}\Lambda_i \qquad (1)$$

Where λ_{im}^{CRW} is the theoretically calculated resonant wavelength, Λ_i is the grating pitch, n_{01}^{co} and n_{1m}^{cl} are the effective refractive indices (ERIs) of the fundamental core mode (LP$_{01}$) and the cladding mode (LP$_{1m}$). The integer i is the number of 40 gratings, and the integer m represents the radial cladding mode order from 2 to 7. Moreover, the ERIs and resonant wavelengths were expressed as a function of fiber parameters, such as the fiber core radius (r_{co}) and the core dopant concentration (C_{GeO2}).
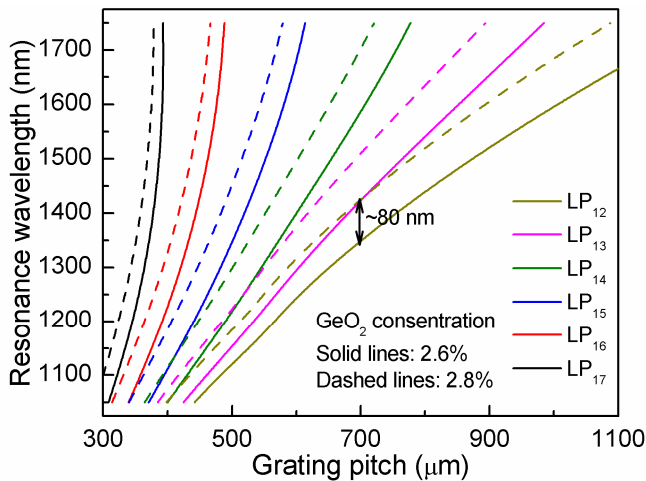

Fig. 3 Simulated phase matching curves at $r_{co} = 4.18$ μm and two different GeO$_2$-concentration $C_{GeO2} = 2.6\%$ and 2.8%.

Generally, the fiber parameters determines the location of resonant wavelengths according to (1). Unfortunately, these fiber parameters are usually unknown, and small deviations of the fiber parameters from the nominal specifications result in significant changes to the resonant wavelength. Fig. 3 illustrates the simulated phase matching curves at $C_{GeO2} = 2.6\%$ and 2.8%, shown as the solid lines and dashed lines. Taking grating pitch of 700 μm for example, a 0.2% change in the germanium dioxide concentration leads to a ~80 nm difference of the resonant wavelength corresponding to LP$_{12}$ mode. Furthermore, the difference increases with the increase of grating pitch and the mode order. In conclusion, a tiny variation in the optical fiber parameters will result in a large difference in the phase matching curves. Therefore, it is difficult to find a direct correspondence between the measured and calculated phase matching curves. Conversely, once some calculated phase matching curves are found to match the measured ones, the optical fiber parameters can be accurately determined.

In this study, we developed a search procedure to find the optical fiber parameters for make the calculated phase matching curves approach the measured ones gradually. In the procedure, we assumed the fiber to have a step-index profile with uniform refractive indices in the cladding and core, where the fiber cladding is pure silica and the fiber core is only doped with germanium dioxide. The RIs of the pure silica cladding and the RIs of the germanium-doped core were calculated using the Sellmeier equation and Fleming's formula [18].

$$n^2 - 1 = \sum_{i=1}^{3} \frac{[SA_i + C_{GeO2}(GA_i - SA_i)]\lambda^2}{\lambda^2 - [Sl_i + C_{GeO2}(Gl_i - Sl_i)]^2} \qquad (2)$$

where SA, Sl, GA, Gl are the Sellmeier coefficients for the SiO$_2$ and GeO$_2$ glasses, respectively, and C_{GeO2} is the dopant concentration of GeO$_2$. On basis of these assumptions, we constructed the following procedure to determine fiber core radius and the germanium dioxide concentration.

The key concept of the procedure is to calculate the theoretical resonant wavelengths and compare them with the measured ones. In order to quantificationally analyze the difference between the measured resonant wavelengths and calculated ones, we defined the average absolute deviation of the resonant wavelengths:

$$D\left(r_{co}, C_{GeO_2}\right) = \frac{1}{N}\sum_{im}\left|\lambda_{im}^{MRW} - \lambda_{im}^{CRW}\right|. \qquad (3)$$

where λ^{MRW} is the measured resonant wavelengths of 40 gratings in Table I, $N = 124$ is the total number of the resonant wavelengths, and λ^{CRW} is the calculated resonant wavelengths we first calculated λ^{CRW} for the presumed optical fiber parameters and fixed 40 fiber grating pitches according to (1), and then compared λ^{CRW} with λ^{MRW} to obtain D according to (3). In order to minimize D, we gradually changed the optical fiber parameters, and repeatedly calculated λ^{CRW} and D. Finally, the optical fiber parameters were determined once D reached a minimal value.

IV. SEARCH PROCEDURE AND RESULTS

Fig. 4 shows the flow chart of the proposed procedure, which includes three-level nested loops. In the first level loop, we fixed both the fiber radius and dopant concentration, and varied the wavelength to calculate the ERIs of the fiber modes. The wavelength varied from 1050 nm to 1750 nm with an interval of 0.1 nm. Such a wavelength range must include the minimal and maximal resonant wavelengths, found in Table I. The ERIs of the fiber modes were calculated using a finite difference method [19, 20]. After obtaining the ERIs at each wavelength, the theoretical resonant wavelengths were calculated according to phase matching condition in (1), in which the grating pitch varied from 360 to 750 μm with an interval of 10 μm. Then the average absolute deviation was calculated by applying (3).

In the second level loop, we fixed the fiber radius and varied the dopant concentration from 2.6% to 2.8% with an interval of 0.01%. At each step, after the dopant concentration had been varied, it was necessary to recalculate the ERIs of fiber modes, the theoretical resonant wavelengths, and the average absolute deviation. In the third level loop, we repeated all of the above calculations only varying fiber core radius from 3.9 to 4.4 μm.
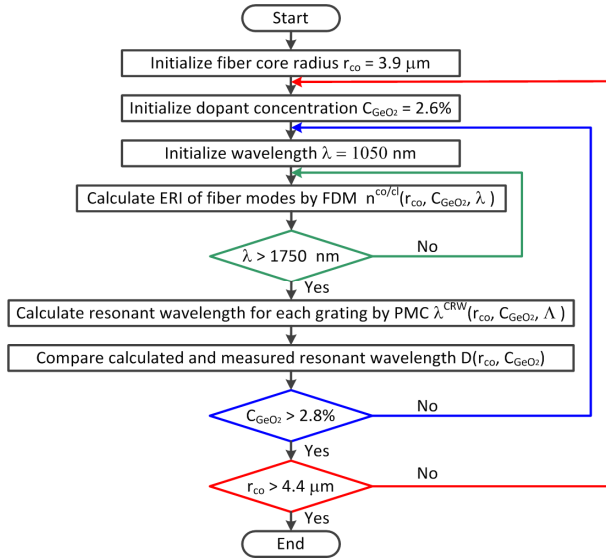
Fig.4 Flow chart of the proposed procedure for reconstructing the fiber parameters. FDM: finite difference method, PMC: phase matching condition.
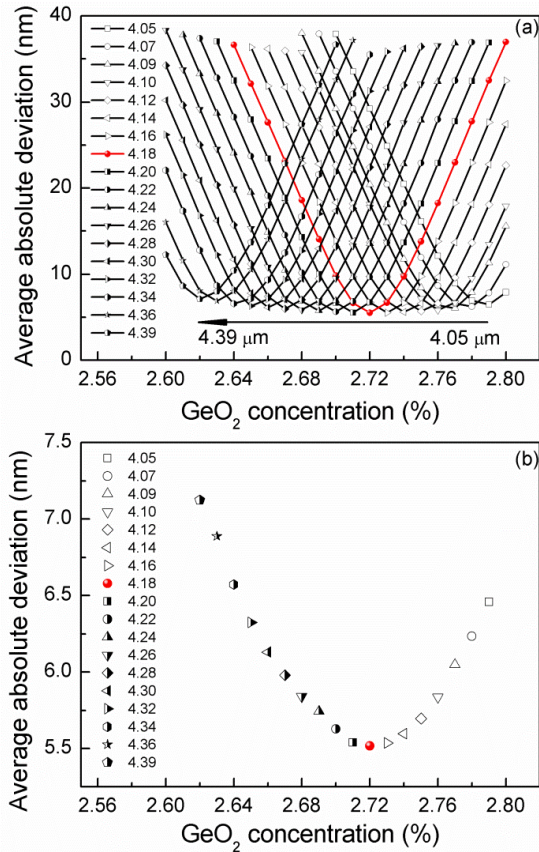

Fig. 5 (a)Average absolute deviation between measured resonant wavelengths and calculated ones,(b)magnified dip of each curve in (a)

After completing the three-level nested loops, we obtained a map of the average absolute deviation, as shown in Fig. 5(a). In this map, each point represented the average absolute deviation at a particular fiber radius and dopant concentration. Each curve represented the variation of the average absolute deviation as function of the dopant concentration at a particular fiber core radius. For good visibility, we have plotted some typical curves in Fig. 5(a).

In Fig. 5(a), it is found the average absolute deviation varied with both the dopant concentration and the fiber core radius, however, there always exists a dopant concentration to minimize the average absolute deviation when the fiber core radius is fixed, exhibiting a dip of each curve in Fig. 5(a). Furthermore, the location of the dip varied with fiber core radius. Fig. 5(b) shows the magnified dip of each curve in Fig. 5(a). It was found that both the dip value of average absolution deviation and the corresponding dopant concentration varied with the fiber core radius. The smallest dip value of D was clearly found to be 5.51 nm. Accordingly, the fiber parameters were determined to be r_{co} = 4.18 µm and C_{GeO2} = 2.72%, respectively.

V. DISCUSSION

To intuitively estimate the correctness of the determined fiber parameters, the theoretical phase matching curves were calculated according to (1) with fiber parameters r_{co} = 4.18 µm and C_{GeO2} = 2.72%; the results were plotted using solid curves in Fig. 2. Comparing the calculated phase matching curves with the previous experimental curves in Fig. 2, the R-squared values were as high as 0.9983, which indicates the determined fiber parameters made the calculated phase matching curves fit well with the experimental curves.

Since fiber core radius and dopant concentration were determined to be r_{co} = 4.18 µm and C_{GeO2} = 2.72%, the wavelength dependence of the refractive indices can be calculated in a large wavelength range according to (2). Consequently, the effective group refractive indices are calculated by use of the following equation:

$$n_g^{co} = n_{01}^{co} - \lambda \frac{dn_{01}^{co}}{d\lambda}. \tag{3}$$

On the other hand, the fiber supplier provided effective group refractive indices at two discrete wavelengths λ = 1310 and 1550 nm. Therefore, it is possible to further verify the correctness of the reconstructed optical fiber parameters by comparing the calculated effective group refractive indices with the nominal ones in the fiber datasheet. The comparison was implemented as shown in Table II. The calculated effective group refractive indices were 1.4661 and 1.4668 at λ = 1310 and 1550 nm, in close proximity to typical values given by the fiber datasheet, i.e., 1.466 and 1.467 [21]. The deviations of the effective group refractive indices was 1×10^{-4} and 8×10^{-4}. Such deviation mainly originated from the arc-discharge induced RI variation. When arc discharge is applied to the fiber, a RI modification is induced by the mechanism of the residual stress relaxation due to the local thermal heating. Some literatures have reported that the arc-discharge induced RI modification is around the order of 10^{-4} [22, 23], which is comparable with the deviation of the effective group refractive indices.

Table II. Effective group refractive indices

Wavelength	Effective group refractive indices	
	Typical values[21]	Calculated values
1310 nm	1.466	1.4661
1550 nm	1.467	1.4668

VI. Conclusion

In conclusion, we constructed a procedure to determine fiber parameters by inscribing LPFGs with different grating pitches. The experimental phase matching curves that corresponded to a group of LP_{1m} cladding modes were obtained after measuring and categorizing the resonant wavelengths of a number of LPFG samples. The phase matching curves were theoretically calculated through solving the ERIs of the core mode and the cladding modes. A procedure was then constructed to search the fiber parameters for ones that minimized the difference between the measured phase matching curves and calculated curves. Finally, the fiber core radius and dopant concentration of a single mode fiber were determined to be 4.18 µm and 2.72%, respectively.

References

[1] B. L. Bachim, T. K. Gaylord, and S. C. Mettler, "Refractive-index profiling of azimuthally asymmetric optical fibers by microinterferometric optical phase tomography," Opt. Lett., vol. 30, no. 10, pp. 1126-1128, 2005/05/15.

[2] W. S. Tsai, S. C. Piao, and P. K. Wei, "Refractive index measurement of optical waveguides using modified end-fire coupling method," Opt. Lett., vol. 36, no. 11, pp. 2008-2010, 2011/06/01.

[3] L. Wang, P. Vaity, B. Ung, Y. Messaddeq, L. A. Rusch, and S. LaRochelle, "Characterization of OAM fibers using fiber Bragg gratings," Opt. Express, vol. 22, no. 13, pp. 15653-15661, 2014/06/30.

[4] S. Ramachandran, S. Golowich, M. F. Yan, E. Monberg, F. V. Dimarcello, J. Fleming, S. Ghalmi, and P. Wisk, "Lifting polarization degeneracy of modes by fiber design: a platform for polarization-insensitive microbend fiber gratings," Opt. Lett., vol. 30, no. 21, pp. 2864-2866, 2005/11/01.

[5] Y. J. Kim, U.-C. Paek, and B. H. Lee, "Measurement of refractive-index variation with temperature by use of long-period fiber gratings," Opt. Lett., vol. 27, no. 15, pp. 1297-1299, 2002/08/01.

[6] C. Schulze, J. Wilde, R. Brüning, S. Schröter, and M. Duparré, "Measurement of effective refractive index differences in multimode optical fibers based on modal decomposition," Opt. Lett., vol. 39, no. 20, pp. 5810-5813, 2014/10/15.

[7] C. Schulze, R. Brüning, S. Schröter, and M. Duparré, "Mode Coupling in Few-Mode Fibers Induced by Mechanical Stress," J. Lightwave Technol., vol. 33, no. 21, pp. 4488-4496, 2015/11/01.

[8] H. M. Presby and I. P. Kaminow, "Binary silica optical fibers: refractive index and profile dispersion measurements," Appl. Opt., vol. 15, no. 12, pp. 3029-3036, 1976/12/01.

[9] G. Yin, J. Tang, C. Liao, and Y. Wang, "Automatic arc discharge technology for inscribing long period fiber gratings," Appl. Opt., vol. 55, no. 14, pp. 3873-3878, 2016.

[10] G. Yin, Y. Wang, C. Liao, J. Zhou, X. Zhong, G. Wang, B. Sun, and J. He, "Long Period Fiber Gratings Inscribed by Periodically Tapering a Fiber," IEEE Photon. Technol. Lett., vol. 26, no. 7, pp. 698-701, Apr 1 2014.

[11] G. Yin, Y. Wang, C. Liao, B. Sun, Y. Liu, S. Liu, Q. Wang, K. Yang, J. Tang, and X. Zhong, "Simultaneous Refractive Index and Temperature Measurement with LPFG and Liquid-Filled PCF," IEEE Photon. Technol. Lett. vol. 26, no. 4, pp. 375-378, 2015.

[12] M. Smietana, W. J. Bock, P. Mikulic, and J. Chen, "Increasing sensitivity of arc-induced long-period gratings—pushing the fabrication technique toward its limits," Meas. Sci. Technol. vol. 22, no. 1, pp. 015201, 2011.

[13] M. Yang, Y. Li, and D. N. Wang, "Long-period fiber gratings fabricated by use of defocused CO_2 laser beam for polarization-dependent loss enhancement," J. Opt. Soc. Am. B, vol. 26, no. 6, pp. 1203-1208, 2009/06/01.

[14] T. Erdogan, "Fiber grating spectra," Lightwave Technology, Journal of, vol. 15, no. 8, pp. 1277-1294, 1997.

[15] A. M. Vengsarkar, P. J. Lemaire, J. B. Judkins, V. Bhatia, T. Erdogan, and J. E. Sipe, "Long-period fiber gratings as band-rejection filters," J. Lightwave Technol., vol. 14, pp. 58-65, 1996.

[16] V. Bhatia, "Applications of long-period gratings to single and multi-parameter sensing," Opt. Express, vol. 4, no. 11, pp. 457-466, 1999/05/24.

[17] X. Shu, L. Zhang, and I. Bennion. "Sensitivity characteristics of long-period fiber gratings." J. of Lightwave Technol., vol. 20, no. 2, pp. 255-266, February, 2002.

[18] J. W. Fleming, "Dispersion in GeO2-SiO2 glasses," Appl. Opt., vol. 23, no. 24, pp. 4486-4493, 1984/12/15.

[19] G. Yin, S. Lou, Q. Li, and H. Zou, "Theory analysis of mode coupling in tilted long period fiber grating based on the full vector complex coupled mode theory," Opt. Laser Technol., vol. 48, pp. 60-66, 2013.

[20] Y. C. Lu, Y. Li, W. P. Huang, and S. S. Jian, "Improved Full-Vector Finite-Difference Complex Mode Solver for Optical Waveguides of Circular Symmetry," J. of Lightwave Technol., vol. 26, no. 13, pp. 1868-1876, 2008.

[21] Yangtze Optical Fiber and Cable Co. *FullBand® Plus Low Loss Single-mode Fiber* http://www.yofc.com.cn/Optical/6/133.aspx

[22] F. Abrishamian, N. Dragomir, and K. Morishita, "Refractive index profile changes caused by arc discharge in long-period fiber gratings fabricated by a point-by-point method," Appl. Opt. vol. 51, no. 34, pp. 8271-8276, December 1 2012.

[23] P. Wang, M. H. Jenkins, and T. K. Gaylord, "Arc-discharge effects on residual stress and refractive index in single-mode optical fibers," Appl. Opt. vol. 55, no. 9, pp. 2451-2456, March 20 2016.

Guolu Yin is a post-doctoral research fellow in the Key Laboratory of Optoelectronic Devices and Systems of Ministry of Education and Guangdong Province, College of Optoelectronic Engineering, Shenzhen University, Shenzhen, China, and is also a visiting research fellow in the Aston Institute of Photonic Technologies, Aston University, Birmingham, U.K. He received the B.S. degree in Optical Information Science and technology, and Ph.D. degree in Electronic Science and Technology from Beijing Jiaotong University, Beijing, China, in 2008 and 2013, respectively. From Dec. 2010 to Jul. 2011, he was in the Department of Physics in the University of Ottawa as a visiting student. He has authored or coauthored more than 30 journal papers. His current research interests focus on optical fiber sensors, long period fiber gratings, and fiber lasers.

Jian Tang is currently working toward the Ph.D. degree in optical engineering in Shenzhen University, Shenzhen, China. Her current research interests include long period fiber gratings and air pressure sensors.

Changrui Liao received the B.S. degree in optical information science and technology and the M.S. degree in physical electronics from the Huazhong University of Science and Technology, Wuhan, China, in 2005 and 2007, respectively, and the Ph.D. degree in electrical engineering from the Hong Kong Polytechnic University, Hung Hom, Hong Kong, in 2012. He is currently with Shenzhen University, Shenzhen, China, as an Assistant Professor. His current research interests include optical fiber sensors and femto second laser micro machining. He has authored or coauthored tenpatent applications and more than 60 journal and conference papers.

Jun He received the B.Eng. degree in electronic science and technology from Wuhan University, Wuhan, China, in 2006, and the Ph.D. degree in electrical engineering from the Institute of Semiconductors, Chinese Academy of Sciences, Beijing, China, in 2011. From 2011 to 2013, he was with Huawei Technologies, Shenzhen, China, as a Research Engineer and worked on performance monitoring for agile optical networks. Since 2013, he has been with Shenzhen University, Shenzhen, China, as a Postdoctoral Research Fellow. His current research interests include optical fiber sensors, fiber Bragg gratings, and optical signal processing. He has authored or coauthored four

patent applications and more than 30 journal and conference papers.

Bing Sun received the B.S. degree in optical information science and technology from Changchun University of Science and Technology, Changchun, China, in 2008, and Ph.D. degree in mechanical engineering from Jiangsu University, Zhenjiang, China, in 2013. Since 2013, he has been with Shenzhen University, Shenzhen, as a Postdoctoral Research Fellow. His current research interests include photonic crystal fiber devices.

Guanjun Wang received the B.S. degree in electronic science and technology and the M.S. degree in physical electronics from Zhengzhou University, Zhengzhou, China, in 2005 and 2008, respectively, and the Ph.D. degree in optical engineering from Beihang University, Beijing, China, in 2012. He was with the North University of China, Taiyuan, China, as a Lecturer, after the graduation. He is currently a Post-Doctoral Researcher with the Institute of Optoelectronic Devices and Systems of Ministry of Education and Guangdong Province, College of Optoelectronic Engineering, Shenzhen University, Shenzhen, China. His research interests include fiber biochemical sensors and fiber grating.

Yiping Wang is a Distinguished Professor and a Pearl River Scholar in the Key Laboratory of Optoelectronic Devices and Systems of Ministry of Education and Guangdong Province, College of Optoelectronic Engineering, Shenzhen University, Shenzhen, China. He was born in Chongqing, China, in July 1, 1971. He received the B.S. degree in Precision Instrument Engineering from Xi'an Institute of Technology, Xi'an, China, in 1995, and the M.S. degree in Precision Instrument and Mechanism and the Ph.D. degree in Optical Engineering from Chongqing University, China, in 2000 and 2003, respectively, where he received the prestigious award of The National Excellent Doctoral Dissertations of China.

In 2003, he joined the Department of Electronics Engineering, Shanghai Jiao Tong University, China, as a postdoctoral research fellow and an associate professor. In 2005, he joined the Department of Electrical Engineering, Hong Kong Polytechnic University, Hong Kong, as a postdoctoral research fellow and a research fellow. In 2007, he joined the Institute of Photonic Technology, Jena, Germany as a Humboldt research fellow. In 2009, he joined the Optoelectronics Research Centre, University of Southampton, U.K. as a Marie Curie Fellow. Since 2012, he has been with Shenzhen University as a Distinguished Professor and a Pearl River Scholar. His current research interests focus on optical fiber sensors, in-fiber gratings, photonic crystal fibers, and fluid-filling technologies. He has authored or coauthored 1 book, 9 patent applications, and more than 130 journal and conference papers with a SCI citation of more than 1000 times.

Dr. Wang is a senior member of IEEE, the Optical Society of America, and the Chinese Optical Society.